IEICE TRANS. INF. & SYST., VOL.E95–D, NO.3 MARCH 2012

PAPER

Correlation-Based Image Reconstruction Methods for Magnetic Particle Imaging

Yasutoshi ISHIHARA[†a)], ***Member***, **Tsuyoshi KUWABARA**[††], **Takumi HONMA**[†], ***and*** **Yohei NAKAGAWA**[†], ***Nonmembers***

SUMMARY Magnetic particle imaging (MPI), in which the nonlinear interaction between internally administered magnetic nanoparticles (MNPs) and electromagnetic waves irradiated from outside of the body is utilized, has attracted attention for its potential to achieve early diagnosis of diseases such as cancer. In MPI, the local magnetic field distribution is scanned, and the magnetization signal from MNPs within a selected region is detected. However, the signal sensitivity and image resolution are degraded by interference from magnetization signals generated by MNPs outside of the selected region, mainly because of imperfections (limited gradients) in the local magnetic field distribution. Here, we propose new methods based on correlation information between the observed signal and the system function—defined as the interaction between the magnetic field distribution and the magnetizing properties of MNPs. We performed numerical analyses and found that, although the images were somewhat blurred, image artifacts could be significantly reduced and accurate images could be reconstructed without the inverse-matrix operation used in conventional image reconstruction methods.

key words: *magnetic particle imaging, MPI, molecular imaging, image reconstruction, correlation, nanoparticles*

1. Introduction

The enhanced permeation and retention (EPR) effect [1], which is caused by the leakage of internally administered nanoparticles from blood vessels and their accumulation in cancerous tissues, can be used to diagnose cancer. Gleich and Weizenecker proposed the magnetic particle imaging (MPI) approach [2], whereby the positions of these magnetic nanoparticles (MNPs) accumulated in cancerous tissue can be detected by applying an alternating magnetic field and local magnetic field from a source positioned outside the body. In basic MPI, this local magnetic field is scanned to encode the spatial information, and the magnetization signal with odd-order harmonics is detected from MNPs within a selected region where the magnetization is not completely saturated by the local magnetic field. An image of the distribution of MNPs is then reconstructed from the signal strength of the odd-order harmonics detected in each place. At this point, however, the system function based on the interaction of the magnetizing properties of MNPs and the applied magnetic field distribution has affected the collected data. Therefore, an image reconstruction method that considers this effect is needed. Gleich *et al*. have proposed image reconstruction methods using the inverse-matrix operation based on a system function [2], [3] and iterative processing [4]. However, when an image matrix becomes large, the use of these methods may result in the reconstructed images being underspecified.

On the other hand, Goodwill and Conolly have formulized an image reconstruction method focused on the scanning speed of a field-free point (FFP), assuming that the system function, based on the interaction between a magnetic field distribution that forms an FFP and the magnetizing properties of MNPs, is linear and space-invariant [5]. However, this method is effective only when MNPs are isolated and the system function is known over the entire reconstruction space.

In all image reconstruction methods, the main reasons for image quality deterioration are that the gradient of the magnetic field distribution that forms a FFP is limited and that the magnetizing properties of MNPs are also imperfect [6]. This is because unnecessary interference signals from MNPs outside the selected region are detected at the same time.

We proposed an image reconstruction method for reducing these interference signals, which are mainly generated as even harmonics [7]–[9]. This was achieved by taking into account the difference between the saturated waveform of the magnetization signal detected from the MNPs within and outside the selected region. We performed numerical analyses to demonstrate that the image resolution in the molecular imaging technique can be improved by using the proposed image reconstruction method based on the abovementioned ideas. Furthermore, a basic system was constructed and the numerical analyses were experimentally validated using MNPs with diameters of 10–50 nm. The detection sensitivity and resolution were improved by the use of methods in the case of locally distributed MNPs. However, a reconstructed image with the correct distribution of MNPs may not be obtained when the MNPs are distributed continuously. This is because the proposed method acts as an intense high-pass filter against the reconstructed image [6], [10].

Here, we propose new methods in order to reconstruct an exact image without artifacts. Our methods are based on the correlation information between the observed signal and a system function, and do not employ the inverse-matrix method.

Manuscript received August 2, 2011.
Manuscript revised November 16, 2011.

[†]The authors are with Meiji University, Kawasaki-shi, 214–8571 Japan.
[††]The author is with Mobil Techno Corporation, Kawasaki-shi, 212–0013 Japan.
a) E-mail: y_ishr@meiji.ac.jp

DOI: 10.1587/transinf.E95.D.872

2. Principles of MPI

2.1 Magnetization Response Generated by an MNP

The static magnetization (M) of an MNP exposed to a magnetic field is described well by the Langevin theory of paramagnetism, which is defined in Eq. (1).

$$M = M_s \left[\coth \frac{m\mu_0 H}{k_B T} - \frac{1}{\frac{m\mu_0 H}{k_B T}} \right] \tag{1}$$

Here, M_s is the saturation magnetization of an MNP, μ_0 is the magnetic permeability of vacuum, m is the magnetic moment of a particle, H is the applied field, k_B is Boltzmann's constant, and T is the absolute temperature [11], [12].

A magnetization response with higher-order harmonics corresponding to the nonlinear magnetization properties of the MNP is generated when an alternating magnetic field is applied to an MNP (Fig. 1, [A]). In contrast, such harmonics are not generated when a local static magnetic field that is strong enough to saturate the magnetization of the MNPs is applied (Fig. 1, [B]). The harmonics can be extracted by Fourier transformation of the detected signals; therefore, the positions of the MNPs can be identified and imaged by scanning the local distribution of a magnetic field with approximately zero strength in the region selected as the FFP but with sufficient strength to saturate the magnetization in non-FFP regions [2].

2.2 Core Components of the MPI System

A conceptual MPI system is shown in Fig. 2 (a). A magnetic field distribution with a very high field strength that surrounds the desired (selected) region, in contrast to having a first-order gradient at the center, is achieved by applying a DC current I_{DC} to a set of Maxwell coil pairs. Thus, an FFP is formed at the center of these coils (Fig. 2 (b)). The position of this FFP is scanned by applying an offset DC current I_{offs} to each coil (Fig. 2 (c)). Note that, in this approach, the shape of the FFP applied to the MNPs has a significant influence on the resolution of the reconstructed image, because the magnetic field distribution formed with the usual magnet is imperfect and not spatially well localized. As described later, under the influence of this factor, an additional signal appears from the MNPs around the boundary of the FFP, and interferes with the signal generated from the MNPs within the FFP.

Here, a magnetization response of MNPs is generated when the alternating magnetic field created by the AC current I_{AC} in one Maxwell coil pair (the top and bottom coils) is applied. Here, the magnetizing properties (saturation characteristics) of the MNP also affect the spatial resolution owing to the finite gradient of the magnetization curve (Fig. 1). Ultimately, the response is detected as an electromotive force (EMF) induced by the receiver coil according to Faraday's law.

2.3 Basic Image Reconstruction Method

As mentioned above, in MPI, image reconstruction is performed with the magnetization response waveform detected while scanning the FFP. In the conventional MPI image reconstruction method, the frequency spectrum of a magnetization response waveform would ideally consist only of odd harmonic components when the FFP is scanned at the point where the MNPs are located. Hence, when the FFP is in the two-dimensional plane (x-z plane in Fig. 2 where $y = 0$), the signal strength in the reconstructed image is expressed by the following equation.

$$F(x, z) = \sum_{n=1}^{N_h} S_{x,z}(2n + 1) \tag{2}$$

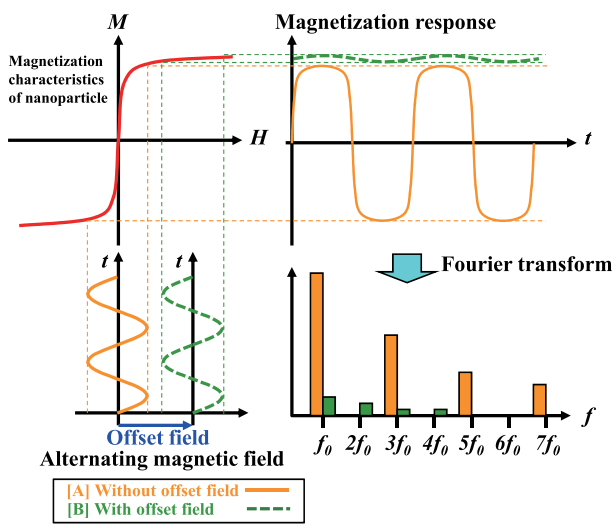

Fig. 1 Principle of MPI.

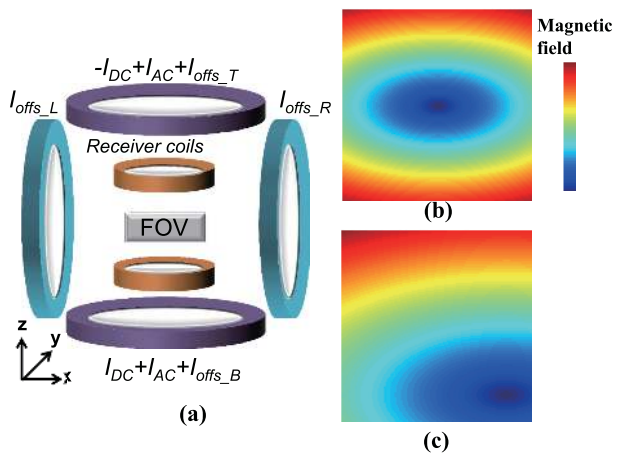

Fig. 2 Basic MPI system. (a) MPI system consists of Maxwell coil pairs and receiver coils. (b) A Maxwell coil pair produces a magnetic field gradient, and an FFP is formed at the center of the field of view (FOV). (c) The position of this FFP can be scanned by adjusting the ratio of currents applied to each coil.

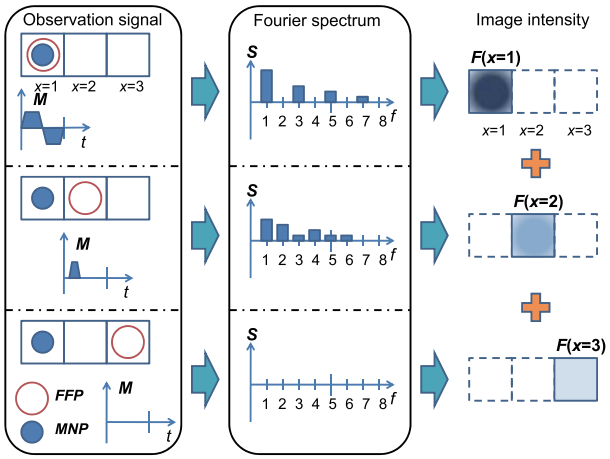

Fig. 3 One-dimensional image reconstruction by the conventional method.

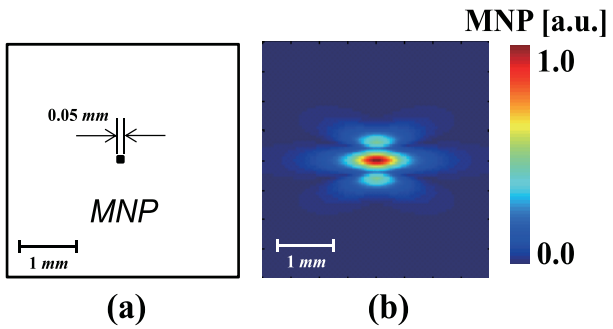

Fig. 4 Image reconstructed by the conventional method. (a) An MNP is set at the center pixel of the FOV as an original image. (b) Image blurring and artifacts in the reconstructed image due to the interference signals by the conventional method.

Here, $F(x, z)$ is the reconstructed image intensity in the x-z plane, $S_{x,z}(n)$ is the n-th harmonic contained in the waveform at each FFP (x, z), and N_h is the maximum harmonic order for reconstruction.

However, since the magnetic field distribution applied to MNPs and the magnetizing properties of an MNP are not ideal, image blurring occurs in the reconstructed result. This situation is explained in the conceptual diagram in Fig. 3. In this figure, the MNP is arranged as a one-dimensional distribution only at the left-end matrix ($x = 1$). When the FFP is scanned on this matrix, only odd-order harmonics are generated and the image distribution is reconstructed according to this signal intensity. Next, when the FFP is scanned on a matrix of $x = 2$, although the detected signal is ideally zero, a magnetization response signal is observed owing to the gently sloped FFP distribution. For this reason, the reconstructed image intensity does not become zero, and even-order harmonics are observed in addition to the odd-order harmonics. Consequently, image blurring occurs despite the extraction of odd-order harmonics by the conventional method. Figure 4 shows an example of such image blurring and artifacts on a reconstructed image.

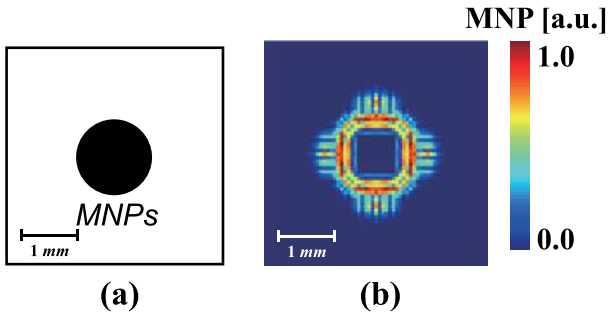

Fig. 5 Problem of image reconstruction by our previous method. (a) MNPs are continuously distributed as an original image. (b) Outer part of the reconstructed image was overemphasized by our previous method.

2.4 Problems with Our Previous Method

From these results, we surmised that the probability that MNPs do not exist at the position where a magnetization response signal with even-order harmonics was detected by the FFP scan was high. In such a case, a correction that emphasizes odd-order harmonics and reduces the even-order harmonics was performed as defined in Eq. (3) [7]–[9].

$$F(x,z) = \sum_{n=1}^{N_h} \left[S_{x,z}(2n+1) e^{\alpha(2n+1)} - k S_{x,z}(2n) e^{\beta(2n)} \right] \quad (3)$$

Here, $F(x, z)$ is the reconstructed image intensity in the x-z plane; $S_{x,z}(n)$ is the n-th harmonic contained in the waveform at each FFP (x, z); N_h is the maximum harmonic order for reconstruction; $\alpha(n)$ and $\beta(n)$ are weighting factors for the harmonics; and k is an arbitrary constant. We demonstrated earlier that the image resolution and detection sensitivity of the MPI can be improved by adjusting the harmonics and distinguishing between the signals generated by MNPs within and outside the FFP. However, when the MNPs are distributed continuously, one problem has been that a reconstructed image turns into a high-pass-filtered image as a result of correcting the interference signal at each point, although the distribution of isolated MNPs can be detected with high sensitivity (Fig. 5).

3. Proposed Methods

In order to overcome this unexpected effect, the following two methods of reconstructing the exact spatial distribution of MNPs are proposed. In these methods, the induced EMF waveform generated from an MNP at each FFP is measured as a system function. The correlation between this system function and an induced EMF waveform generated by the distribution of the unknown MNPs at each FFP is then calculated without any inverse matrix operation.

3.1 Proposed Method–1

In the first method, the estimation of the distribution of

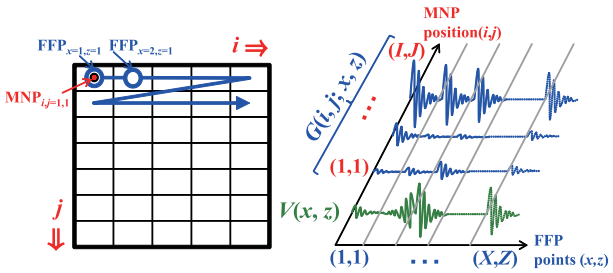

Fig. 6 Concept of system function for the proposed method–1.

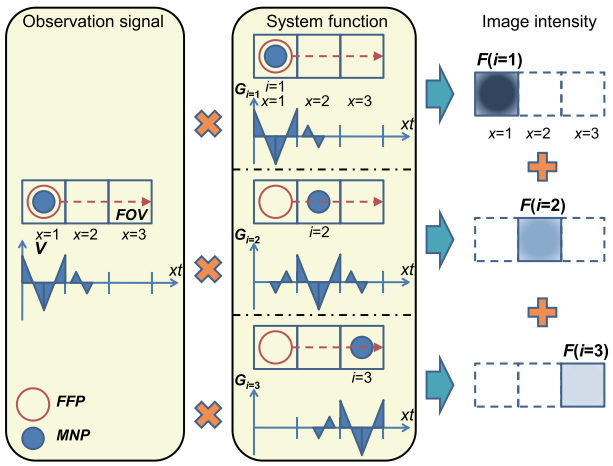

Fig. 7 One-dimensional image reconstruction by the proposed method–1.

MNPs is based on the correlation between the observed signal $V_{x,z}(t)$ from the distribution of unknown MNPs and the system function (*i.e.*, the point-spread function), $G_{i,j;x,z}(t)$, which is a space-variant system determined by the interaction of the magnetic field and the distribution of MNPs. As shown in Fig. 6, this system function can be determined by measuring the waveforms at the FFP points of (x, z) when an MNP is set at each point (i, j) within the field of view (FOV), and by connecting all of these measured waveforms as one-dimensional data sequentially arranged in an array of rows and columns (x, z) and expressed as Eq. (4).

$$G_{i,j;x,z}(t) \equiv G_{i,j}[xt + X(z-1)] \quad (x = 1, 2, \cdots, X),\ (z = 1, 2, \cdots, Z) \tag{4}$$

Similarly, the observed signal $V_{x,z}(t)$ is also expressed as Eq. (5).

$$V_{x,z}(t) \equiv V[xt + X(z-1)] \quad (x = 1, 2, \cdots, X),\ (z = 1, 2, \cdots, Z) \tag{5}$$

Consequently, the MNP distribution $F(i, j)$ in the x-z plane is reconstructed using Eq. (6).

$$F(i, j) = \int V_{x,z}(t) G_{i,j;x,z}(t) dt \tag{6}$$

To be specific, the method of reconstructing one-dimensional distribution is explained in Fig. 7 in relation to Fig. 3. Here, it is assumed that an MNP exists in the left-end matrix. A signal is observed by scanning the FFP in each position (x = 1, 2, 3) (left column in Fig. 7). The signal series observed at the position of each FFP is arranged in order in the direction of the time-axis, and is made into the one signal series $V_x(t)$ (left column in Fig. 7). In contrast, a system function is determined from the signal detected by scanning the FFP (x = 1, 2, 3), when one MNP has been arranged in each position (i = 1, 2, 3) corresponding to the matrix position of the reconstructed image, as shown in the central column in Fig. 7. That is, the signal acquired by scanning the FFP from x = 1 to 3 is arranged in the direction of the time-axis, and is made into one signal sequence $G_{i;x}(t)$. Here, the system function in the case that an MNP has been arranged at the left end (i = 1) is expressed as $G_{i=1;x}(t)$. Similarly, the system function $G_{i=2;x}(t)$, which scans the FFP from x = 1 to 3, is defined when an MNP is arranged at i = 2.

A reconstructed image $F(i)$ is expressed as the sum of each correlation between the observation signal $V_x(t)$ and the system function $G_{i=1,2,3;x}(t)$. In this way, it is possible to estimate the position of an MNP.

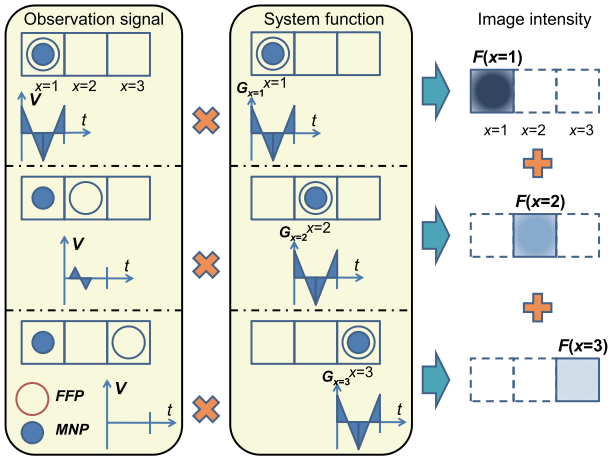

Fig. 8 One-dimensional image reconstruction by the proposed method–2.

3.2 Proposed Method–2

A second method for improving spatial resolution was attempted. In this method as well, the signals are generated from MNPs outside an FFP region owing to the imperfection of the system described above. However, only the signal generated from an MNP set in the FFP region is taken into consideration as a system function.

The concept of image reconstruction in this method is shown in Fig. 8. As in the first method, a procedure that reconstructs the one-dimensional MNP distribution is addressed. When an MNP exists in the left-end matrix, the FFP is scanned for every matrix and a signal is observed as $V_x(t)$ at each FFP (left column in Fig. 8). The system function is defined as the signal generated when an MNP has been arranged at each matrix and the FFP is scanned at the corresponding matrices (central column in Fig. 8). This is

equivalent to assuming that a signal is not generated when the FFP is scanned at other matrices. The system function is then expressed as $G_x(t)$. The intensity of a reconstructed image is obtained by calculating the correlation between the observation signal and the system function at each position.

Consequently, the MNP distribution $F(x, z)$ in the x-z plane is reconstructed using Eq. (7).

$$F(x,z) = \int V_{x,z}(t) G_{x,z}(t) dt \tag{7}$$

Thus, compared to the abovementioned method–1, a suppression of image blurring arising from the imperfection of the FFP is expected by using an ideal system function (that is, where the interference signal is ignored).

4. Numerical Simulation

4.1 Simulation Methods

In order to examine the validity of the proposed methods based on the concept of correlations between the observed signals and system functions, a numerical analysis was performed with the system model shown in Fig. 2. In this examination, two coil pairs (diameter: 0.5 m, distance: 1.0 m) and a receiver coil (diameter: 0.1 m, number of turns: 1) were used, and the FOV was set to $4 \times 4\,\mathrm{mm}^2$ with a matrix size of 81×81. A magnetic field distribution with a gradient field of about 2.5 T/m formed in the z direction at MNPs with a particle diameter of 50 nm was applied as an FFP with this coil pair. In addition, an alternating magnetic field of 1 mT was applied at a frequency of 35 Hz in the same direction.

4.2 Simulation Results

Figure 9 (a) shows two original images. The left panel indicates an MNP distributed at a central pixel ($0.05 \times 0.05\,\mathrm{mm}^2$) and the right panel indicates MNPs distributed in the shape of a square ($1.0 \times 1.0\,\mathrm{mm}^2$). Figure 9 also shows the corresponding, images reconstructed by the conventional method (b), the proposed method–1 (c), and the proposed method–2 (d). With the conventional method, the reconstructed distribution was spread around the region where the MNPs were actually positioned, and image artifacts were observed. In contrast, the images for the proposed methods confirm that compared to the conventional method, image artifacts could be drastically reduced. Figure 10 shows the profile of each central section of the image reconstructed by each method in the case that an MNP is arranged at the central pixel of FOV in Fig. 9. As mentioned above, the side lobes (image artifacts) due to the interference signal are suppressed with each of the proposed methods.

For signal profiles shown in Fig. 10, it is difficult to evaluate the image resolution by using the full width at half maximum. Here, based on the same idea as that of the standard deviation in a Gaussian distribution, the range in which the integrated value of the image intensity was equivalent to

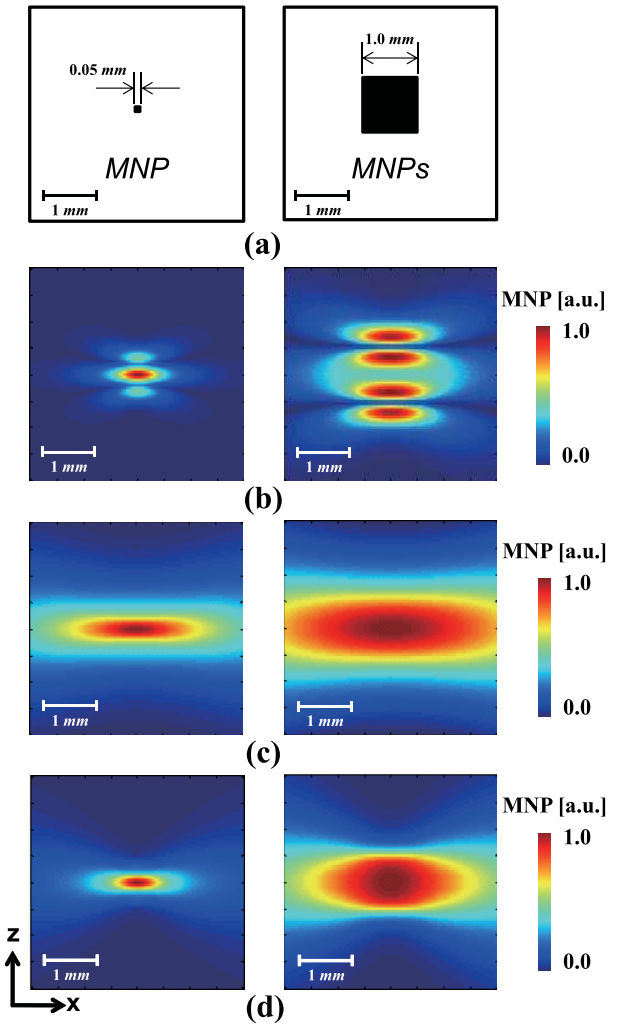

Fig. 9 Image reconstructed by each method. (a) Original images. (b) Images reconstructed by the conventional method. (c) Images reconstructed by the proposed method–1. (d) Images reconstructed by the proposed method–2. The left panels indicate images when MNP is distributed at a central pixel. The right panels indicate images when MNPs are distributed in the shape of a square.

$\pm 1\sigma$ from the center of the image was defined as the image resolution. Based on these criteria, the image resolutions (2σ) in the z direction for the conventional method, the proposed method–1, and the proposed method–2 were 0.5, 1.0, and 0.3 mm, respectively. In addition, the corresponding image resolutions in the x direction were 0.9, 2.3, and 1.6 mm, respectively.

5. Discussion

5.1 Causes of Image Blurring and Countermeasures

It was confirmed with numerical analyses that the image artifacts observed in the conventional method do not appear with the proposed image reconstruction methods, especially with method–2. However, it was shown that the image resolution along the x direction deteriorates even with method–2

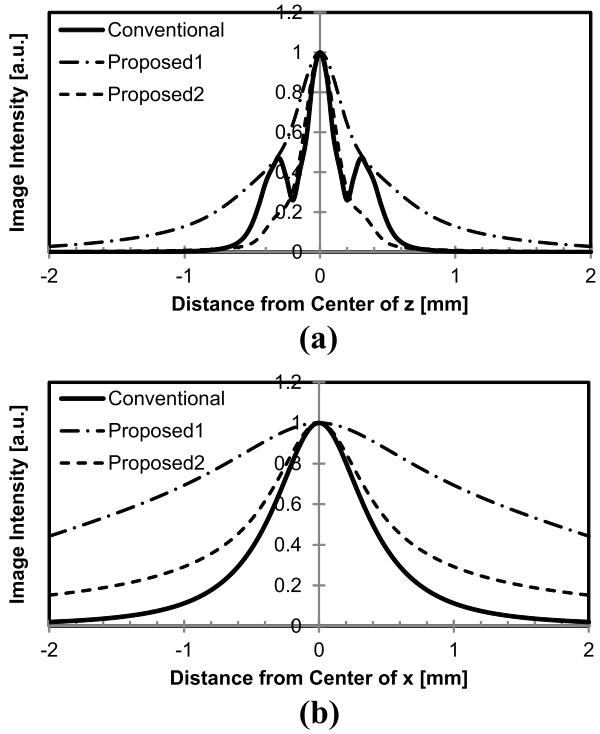

Fig. 10 Image profile along two axes. These correspond to the profile in the case that the MNP is arranged at the central pixel of the FOV in Fig. 9.

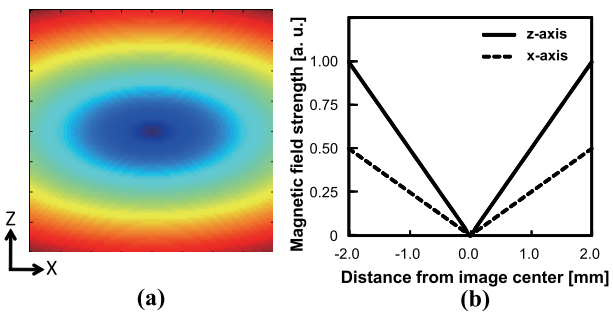

Fig. 11 Magnetic field distribution of Maxwell coil pair. (a) Distribution of FFP formed with a Maxwell coil pair. (b) Profile of FFP distribution along each axis.

(compared to the size of the MNP distribution in an original image (0.05 mm), the degradation of image resolution is about 30 times as great.), although that along the z direction is improved. Here, the cause of image blurring is considered.

One of the main reasons is that a relatively gentle and ellipse-like magnetic field distribution is formed with a normal Maxwell coil pair (Fig. 11 (a)). Namely, the magnetic field intensity required to saturate an MNP magnetically near the FFP is not obtained, and an interference signal is generated. In particular, the magnetic field intensity along the x direction is half that along the z direction (Fig. 11 (b)).

Furthermore, note that differences in the application directions of a gradient magnetic field (x- and z-axes) and an alternating magnetic field (z-axis) change the waveform of

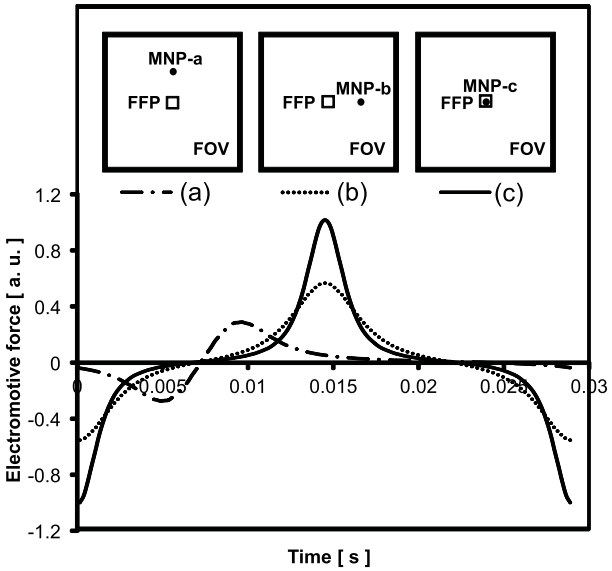

Fig. 12 Waveforms of EMF depending on magnetic field components.

the generated EMF. Figure 12 (a) shows the condition in which an MNP was set at position MNP-a, and the FFP was scanned at the center of the FOV. Under these conditions, the magnetic field intensity at MNP-a approximately consists of only the z component. When an alternating magnetic field is superimposed on the MNP at MNP-a (far from the center along the z direction), the MNP experiences a magnetic field intensity that is a scalar sum of the alternating and gradient magnetic fields. This is because the magnetic field component of the alternating field is composed approximately of the z component. In this case, the "asymmetry" of the induced EMF wave (Fig. 12 (a)) (*i.e.*, the interference signal generated from an MNP) is intensified, and its correlation with the induced EMF wave obtained from the selected region corresponding to the system function (Fig. 12 (c)) decreases. Therefore, the observed interference signals are suppressed in images reconstructed by the proposed methods, and a high image resolution about the z-axis is expected.

In contrast, Fig. 12 (b) shows a condition in which an MNP was set at position MNP-b (far from the center along the x direction), and the FFP was scanned in the center of the FOV. Under these conditions, the magnetic field intensity at MNP-b approximately consists of only the x component. When an alternating magnetic field is superimposed on the MNP, the induced-EMF wave observed with a receiver coil is similar to the system function. Therefore, the correlation of the induced EMF wave of an interference signal (Fig. 12 (b)) and that corresponding to the system function (Fig. 12 (c)) obtained from the selected region increases. Therefore, it becomes difficult to suppress the observed interference signal by the proposed methods, and the image resolution about the x-axis decreases. The proposed method–1 is particularly affected by this process because the correlation is calculated after the signal observed by each FFP is arranged. Consequently, image blurring in

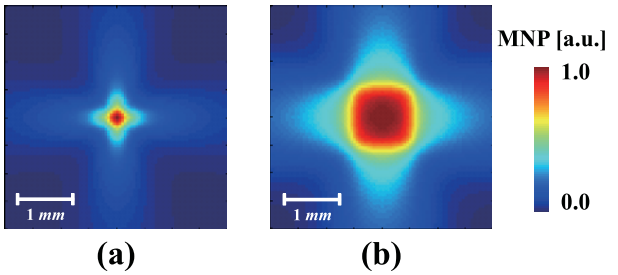

Fig. 13 Improvement in image blurring by superimposing two acquired images with changes in the direction of a magnetic field. The original images correspond to Fig. 9 (a).

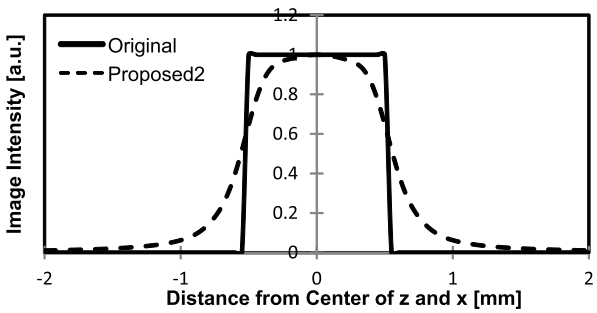

Fig. 14 Image profiles along the two axes corresponding to those in Fig. 13 (b).

the proposed method–1 becomes large compared to that in the proposed method–2.

In order to improve image resolution, it is necessary to suppress such image blurring. One solution is to add each reconstructed image obtained by exchanging the direction of the gradient magnetic field components that form the FFP and received signal components. Figure 13 shows images reconstructed by the abovementioned method when MNPs were arranged in positions corresponding to those in Fig. 9 (a). It was confirmed that the spread of image blurring along the x-axis is improved by superimposing two acquired images with changes in the direction of the magnetic field. From Fig. 13 (a), the image resolutions about the x-axis and z-axis were both 0.54 mm. In addition, the outlines became clearer in the reconstructed image shown in Fig. 13 (b) than in the image shown in the right panel of Fig. 9 (d). Although the image resolution improved, image blurring was recognized when the profile was compared to that of the original image, as shown in Fig. 14.

5.2 Validity of Simulation Methods

In order to confirm the validity of these numerical analysis procedures, a prototype system that collects one-dimensional MPI image data was constructed [6]. In the experiment, FFP was formed with a gradient magnetic field of 1.2 T/m by a Maxwell coil pair (diameter: 180 mm, number of turns: 285 each, opposite distance: 30–50 mm). The magnetization response waveform generated from the MNPs at the center of the Maxwell coil pair was detected with a receiver coil (diameter: 35 mm, number of turns: 40) that surrounds the MNPs when an alternating magnetic field with an amplitude of 90 mT (frequency of 35 Hz) was applied. The MNPs consisted of 2.0-g of dry iron oxide particles with a nominal diameter of 10 nm (EMG1500, Ferrotec Corp., Chiba, Japan). By comparing normalized magnetization signals obtained under the same conditions by numerical analysis and experiment, the error in amplitude between the simulated and experimental signals was found to be 5% or less. Moreover, a comparison of the third-order harmonic components confirmed that both were in agreement with an accuracy of about 80%. Accordingly, the numerical analyses in this study were shown to be appropriate.

6. Conclusions

In MPI, interference of the magnetization signal generated by the MNPs outside an FFP, owing to their nonlinear responses, leads to degradation of the image resolution. We therefore proposed new methods based on the correlation between the observed signal and a system function, and performed numerical analyses. Although image blurring was still evident in the numerical analyses, we showed that image artifacts could be drastically reduced compared to the conventional method. Although further improvement of image quality is necessary, these methods can be used for image reconstruction without the inverse-matrix operation in conventional methods.

Acknowledgments

This study was supported by a Grant-in-Aid for Scientific Research (B), 20300155, 2008 from the Japan Society for the Promotion of Science (JSPS).

References

[1] Y. Matsumura and H. Maeda, "A new concept for macromolecular therapeutics in cancer chemotherapy: Mechanism of tumoritropic accumulation of proteins and the antitumor agent smancs," Cancer Res., vol.70, no.12, pp.6387–6392, Dec. 1986.
[2] B. Gleich and J. Weizenecker, "Tomographic imaging using the nonlinear response of magnetic particles," Nature, vol.435, no.7046, pp.1214–1217, June 2005.
[3] J. Weizenecker, J. Borgert, and B. Gleich, "A simulation study on the resolution and sensitivity of magnetic particle imaging," Phys. Med. Biol., vol.52, no.21, pp.6363–6374, Nov. 2007.
[4] J. Weizenecker, B. Gleich, J. Rahmer, H. Dahnke, and J. Borgert, "Three-dimensional real-time in vivo magnetic particle imaging," Phys. Med. Biol., vol.54, no.5, pp.L1–L10, March 2009.
[5] P.W. Goodwill and S.M. Conolly, "The X-Space formulation of the magnetic particle imaging process: 1-D signal, resolution, bandwidth, SNR, SAR, and magnetostimulation," IEEE Trans. Med. Imaging, vol.29, no.11, pp.1851–1859, Nov. 2010.
[6] Y. Ishihara, T. Kuwabara, and N. Wadamori, "Image resolution and sensitivity improvements of a molecular imaging technique based on magnetic nanoparticles," in Electromagnetic Waves, ed. V. Zhurbenko, pp.493–510, InTech, Rijeka, 2011.
[7] Y. Kusayama and Y. Ishihara, "A preliminary study on the molecular imaging device using magnetic nanoparticles," IEICE Technical Report, MBE2007-48, Sept. 2007.

[8] Y. Ishihara and Y. Kusayama, "Resolution improvement of the molecular imaging technique based on magnetic nanoparticles," Proc. SPIE, vol.7258, pp.72584I.1–72584I.8, Feb. 2009.
[9] Y. Kusayama and Y. Ishihara, "High-resolution image reconstruction method on the molecular imaging using magnetic nanoparticles," IEICE Trans. Inf. & Syst. (Japanese Edition), vol.J92-D, no.9, pp.1653–1662, Sept. 2009.
[10] Y. Ishihara, T. Kuwabara, and N. Wadamori, "Sensitivity improvement of a molecular imaging technique based on magnetic nanoparticles," Proc. SPIE, vol.7965, pp.79652J.1–79652J.8, Feb. 2011.
[11] L. Vekas, M. Rasa, and D. Bica, "Physical properties of magnetic fluids and nanoparticles from magnetic and magneto-rheological measurements," J. Colloid Interface Sci., vol.231, no.2, pp.247–254, Nov. 2000.
[12] C.T. Yavuz, J.T. Mayo, W.W. Yu, A. Prakash, J.C. Falkner, S. Yean, L. Cong, H.J. Shipley, A. Kan, M. Tomson, D. Natelson, and V.L. Colvin, "Low-field magnetic separation of monodisperse Fe_3O_4 nanocrystals," Science, vol.314, no.5801, pp.964–967, Nov. 2006.

Yasutoshi Ishihara received his B.E. and M.E. degrees in electrical and electronic systems engineering and the Ph.D. degree in information science and control engineering in 1987, 1989, and 2002, respectively, from the Nagaoka University of Technology, Niigata, Japan. He is currently an associate professor at the School of Science and Technology, Meiji University. He worked at Toshiba Co., Ltd., Kawasaki, Japan from 1989 to 2004, and the Department of Electrical Engineering, Nagaoka University of Technology, Nagaoka, Japan from 2004 to 2009. His research interests include image processing, image recognition, diagnostic imaging systems, and noninvasive cancer treatment systems.

Tsuyoshi Kuwabara received his B.E. and M.E. degrees in electrical, electronics, and information engineering from the Nagaoka University of Technology in 2008 and 2010, respectively. He joined Mobil Techno Corporation, Kawasaki, Japan, in April 2010. His research interests include image processing and mobile communication systems.

Takumi Honma has been studying at the School of Science and Technology, Meiji University. His research interests are in molecular imaging systems based on magnetic nanoparticles.

Yohei Nakagawa received his B.E. degree in mechanical engineering informatics from Meiji University in 2010. Since 2010, he has been studying at the Graduate School of Science and Technology, Meiji University. His research interests include noninvasive measurement and diagnostic imaging systems.